Geochemical Transactions

RESEARCH Open Access

Development of a kinetic-thermodynamic model for lime-stabilization of Na-bentonite

Tasneem Ahmadullah[1*] and Maria Chrysochoou[2]

Abstract

This study presents the first kinetic model to predict the solid and pore solution composition of Na-bentonite clay reacting with slaked lime over a period of 720 days. The model successfully accounts for most experimental data using a single kinetic rate constant. The following sequence of reactions was predicted by the model: initial rapid dissolution of portlandite within the first 7 days, leading to a decrease in pH and dissolved calcium, and concurrent formation of calcium silicate hydrates (C-S-H: jennite), calcium aluminate hydrate (C-A-H: C_4AH_{13}), calcium aluminosilicate hydrates (stratlingite) and hydrotalcite. After 7 days, jennite and stratlingite are predicted to transform into tobermorite-II, contributing to strength development up to 28 days. From 28 to 90 days, continued montmorillonite dissolution is predicted, along with minor formation of ettringite, partial tobermorite-II dissolution, and precipitation of secondary phases such as albite and talc. Experimentally, portlandite dissolution was confirmed by TGA and XRD and found to be complete within 7 days, in agreement with model predictions. However, other predicted solid-phase transformations (e.g., tobermorite-II formation and dissolution, ettringite, albite, and talc formation) could not be conclusively verified through experimental techniques. Aqueous phase measurements confirmed that the pH and Ca trends in solution, and that equilibrium was reached by 90 days.

Keywords Lime stabilization, Geochemical modeling, Chemical kinetics, Na-bentonite, Pozzolanic reaction

Introduction

Mixing of clay soils with cementitious materials, such as lime, Portland cement and other pozzolans has a long history and multiple applications, including stabilization of clay subgrades in road construction [31, 42], stabilization/solidification of contaminated soils [19], construction of clay barriers for radioactive waste storage [16], CO_2 storage sites [24] and design of blended cements with sustainable materials and targeted properties [43]. Given the significant variability that clay soils present in terms of composition, geomechanical properties and reactivity [18], there is a large body of literature studying the behavior of treated clays over time. Most studies focus on the mechanical properties (strength, compressibility, expansion) that are of practical interest, but many also include qualitative information on the evolution of the mineralogy and microstructure that drive the observed changes in behavior [4, 13, 40].

Early studies on lime treatment of clays [17, 22, 32, 36] established the reactions that cause changes in geotechnical properties; initially, cation exchange and flocculation improve workability by reducing soil plasticity, followed by pozzolanic reactions that form Calcium Silicate Hydrates (C-S-H), Calcium Aluminate Hydrates (C-A-H) and Calcium Aluminate Silicate Hydrates (C-A-S-H), providing long term strength. The composition of the C-S-H, C-A-H and C-A-S-H products varies to some extent with time, clay mineralogy and type of pozzolan

*Correspondence:
Tasneem Ahmadullah
tasneem.ahmadullah@pnnl.gov
[1]Pacific Northwest National Laboratory, Richland, WA 99354, USA
[2]College of Engineering, University of Missouri, Columbia, MO 65211, USA

added. Tobermorite gel is reported to be the primary C-S-H phase formed [10] and various C-A-H phases have been reported, including C_3AH_6, C_4AH_{13}, CAH_{11}, CAH_{10} as well as sulfate-bearing monosulfate and ettringite [10, 26, 35].

With the advancement of molecular analysis techniques, research expanded into quantifying clay/lime pozzolanic reactions and linking those to strength development over time both for non-expansive [14, 35, 44, 45] and expansive clays [7, 11, 47]. A few studies developed geochemical models [3, 5, 15] to describe the reactions of clay minerals with lime. De Windt et al. [15] presented a kinetic model on Ca-bentonite and lime interactions for a curing time of 98 days, utilizing a combination of spectroscopic analyses (X-ray Diffraction (XRD), Thermogravimetric Analysis (TGA) and Nuclear Magnetic Resonance (NMR)) and batch leaching tests to evaluate the pore solution composition of the mixed clay. Akula et al. [5]'s equilibrium model on expansive clays with plasticity index > 45% assessed the domination of durable C-S-H (pozzolanic) reactions over a combination of cation exchange and pozzolanic reactions in the clay soil stabilization process. An equilibrium model by definition predicts composition under thermodynamically stable conditions and is thus useful to evaluate long-term system performance but cannot provide phase evolution in a chemically dynamic system.

These approaches are similar to those used in the cement and concrete literature, with one critical difference: the extraction and direct measurement of pore solution composition, which provides a more accurate representation of the system's chemical evolution. Various methods have been developed for pore solution extraction of cement and concrete and significant advances have been made in the thermodynamic and kinetic modeling of blended cements [48]. However, a gap remains in obtaining experimental pore solution data and developing quantitative kinetic models to describe and predict the long-term reactions of lime-stabilized clays. In a previous study, we developed a kinetic model for a lime-kaolinite system with pure kaolinite as the single-phase present [1]. The current study presents a similar approach of utilizing mineralogical and pore solution extraction analyses to validate a kinetic model for a lime-bentonite system that is more complex and includes multiple minerals.

Table 1 Atterberg limits and chemical composition (in wt %) of Na-bentonite

Clay	Bentonite
Liquid Limit	384
Plastic Limit	68
SiO_2	66.266
Al_2O_3	21.056
Na_2O	2.550
Fe_2O_3	4.792
P_2O_5	0.054
SO_3	0.562
K_2O	0.738
MgO	1.824
CaO	1.734

Materials and methods

Materials

Wyoming sodium bentonite was obtained from Bentonite Performance Minerals (product BARA-KADE). The Atterberg limits and chemical composition of the material determined by X-Ray Fluorescence (XRF) are shown in Table 1, and hydrometer test data along with mineralogy of the material determined by X-Ray Diffraction (XRD) are shown in Supporting Information (Figure S1 and Figure S2), available online. Based on the particle size distribution (particles below 2 µm) and the qualitative XRD analysis conducted for each fraction size, it was estimated that, the Na-bentonite comprises 80% Na-montmorillonite and approximately 20% by weight of accessory minerals, including quartz (SiO_2), cristobalite (SiO_2), a mixed feldspar (anorthite-albite solid solution), muscovite mica and zeolite (Na-clinoptilolite). This composition resembles the SWy-2 smectite of the source clays of the Clay Minerals Society analyzed by [12]. The Na-montmorillonite reflections appear in the same locations, corresponding to d-spacings of 8, 4.5, 3.2, 2.5, 1.7 and 1.5 Å. The cation exchange capacity was measured at 85 meq/100 g and analysis of the resulting pore solution yielded a mixture of Na (80%) and Ca (10%) along with the presence of Mg (0.4%) and K (0.17%). Slaked lime was obtained from Fisher Scientific which contained 95% $Ca(OH)_2$ (ACS grade).

Experimental methods

Standard Proctor compaction curves and 7-day UCS analyses of Na-bentonite mixed with 5% SL were performed according to ASTM methods(ASTM 2021) and (ASTM 2017), respectively, and used to determine the moisture content for long term studies. As discussed in Ahmadullah Tasneem & Chrysochoou Maria, [2], the results showed that bentonite mixed with 5% slaked lime had a flat compaction curve with an optimum moisture content around 30%, while UCS studies conducted with 5% and 8% lime showed that strength was higher at moisture contents above the optimum (35–45% range), with no clear maximum At contents below 35%, the mixtures were too dry and stiff to be practically workable, and above 45%, they become overly wet and difficult to work with.

These findings were assessed in the context of previous studies. Bell [10] observed that peak strength is typically achieved just above the OMC, while Maubec et al. [35] used a slightly lower target at 98.5% of OMC. The National Lime Association recommends preparing samples within ± 1% of OMC. Taking all these considerations into account along with the practical workability of the material, a final selection of 8% SL and 40% moisture content was made for long term sample preparation. All subsequent experimental analysis including solid phase characterization (XRD, TGA and NMR) and liquid phase analysis were conducted on the samples prepared with this composition.

Quadruplicate specimens were prepared for thirteen curing times (0, 1, 3, 5, 7, 28, 90, 120, 270, 360, 540 and 720 days), sealed tightly and cured at room temperature and ± 96% relative humidity. Table S1 summarizes all tests performed on the samples.

At each curing time, the samples were removed from storage, checked for integrity and tested for UCS. Subsamples from the UCS sample breaks were used for solid and liquid analyses. Sample breaks were collected from the core of the compacted sample after discarding the outer layer that was more prone to drying and carbonation. Adopting the approach of Lothenbach and Winnefeld [33], acetone drying was originally adopted for solid analysis; however, similar to the observations of Weise et al. [49], residual acetone peaks remained in TGA spectra, while isopropyl alcohol (IPA) was observed to result in improved resolution for both TGA and XRD. 10 g of the sample was mixed with 40 mL of a drying agent and the mixture was shaken for an hour. When acetone was used, air drying for 24 h was sufficient to obtain a dry sample for NMR spectra; however, for TGA and XRD mixed with IPA it was necessary to oven dry at 80°C to completely remove IPA from the clay particles. While this may have an impact on the stability of hydrates such as ettringite, it was the only drying method that yielded a dry material with sufficient spectra resolution.

Additional paste studies were conducted on specimens mixed with 8% and 15% SL at 40% moisture content, sealed in double plastic bags at room temperature. Samples were obtained, dried with isopropanol and subjected to TGA and XRD testing for times between 4 h and 14 days.

Thermogravimetric analysis was performed at UConn's Institute of Material Science using TGA Q500. For the analyses the samples were heated up to 1000˚C at a rate of 5˚C/min in an argon atmosphere. The thermograms were analyzed using the Universal Analysis software. The software employs Gaussian or Lorentzian peak fitting methods to generate the derivative of the thermograms.

A Bruker Advance III 400 MHz solid state NMR spectrometer was used for NMR analysis. Using Magic Angle Spinning (MAS) technique, the solid samples were analyzed for ^{29}Si and ^{27}Al at frequencies 79 and 107 MHz respectively. The chemical shifts in the samples were referred to tri(trimethyl-silyl)silyl (TTMS). The spectra were deconvoluted and integrated using the OriginPro software.

For XRD analysis, a Bruker D2 phaser diffractometer with slit size 1 × 10 mm, CuK_α ($\lambda = 1.54$ nm) radiation and a step size of 0.01°. The two-theta range of the analyses was 5 to 65°. For two theta calibration, 20% corundum (Al_2O_3) was used as internal standard. The Jade software v. 8.5 (Materials data Inc) was used for qualitative analysis with reference to the International Crystal Structure Database.

For liquid analysis, a portion of UCS breaks from bentonite-lime cured samples was used to extract pore water using the custom-made extraction apparatus described in (Ahmadullah Tasneem & Chrysochoou Maria, 2022). Pore water extraction from bentonite was challenging because of its low permeability and high plasticity, so that only a fraction of the total free water can be extracted [20]. The typical timeline to extract pore water from bentonite compacted samples is weeks and even months [20, 37]. However, this study required short-term water recovery to capture the solution at each curing time, restricting the squeezing time to hours. A squeezing test up to 5 h under an applied force of 10^6 to 2×10^6 lbs yielded 4 mL of free water from 300 g bentonite sample compacted with 8% lime and 40% water; the extracted water was subsequently filtered through 0.45 µm. It was observed that increasing the applied load or prolonging the exposure did not result in increased recovery, increasing the load resulting in the bentonite mixture plugging the tubing and contaminating the extracted pore water. The low amount of recovered water limited the ability to conduct analysis of the recovered solution. This issue may be mitigated by conducting multiple solution extraction tests using sub-specimens of the same UCS break and combining the extracted pore water. This was done for a few samples as needed but was not consistently possible due to the practical limitations of the time and effort required to perform all described analyses for quadruplicate samples within a short time frame.

The pH was measured in the original solution using a micro-electrode, which enables accurate measurements for small volumes. A Shimadzu Total Organic Carbon (TOC) analyzer was used for inorganic carbon analysis and a Thermo-Fisher UV-visible spectrophotometer was used for silica analysis following method ASTM D859-16, both in the original solution. The remaining solution was then diluted with DI water 50 to 100 times for further analysis. This approach increased the detection limit of all analyses, causing certain elements such as Fe and Mg to not be detectable at any curing time.

Metals (Na, K, Ca, Mg, Fe and Al) in the liquid samples were analyzed via ICP-MS, and SO_4^{2-} via Ion

Table 2 Kinetic rate parameters for montmorillonite [34]

Phases	log k_{25}^{nu}	log k_{25}^{H}	log k_{25}^{OH}	n_H	n_{OH}
Montmorillonite	-14.032	-10	-10.6	0.69	0.34
Gypsum	-3.19				

Chromatography by a certified laboratory (Phoenix Environmental Laboratories, Manchester, CT).

Model setup and parameters

The bentonite-lime model was set up using the PHREEQC software [39] and according to Transition State Theory [29] simplified to the following equation,

$$r = A_{min}(k_{25}^{nu} + k_{25}^{H}a_{H}^{nH} + k_{25}^{OH}a_{OH}^{nOH})(1 - \frac{IAP}{K}) \quad (1)$$

where A_{min} is the reactive surface area of the mineral [m^2], k_{25}^{nu} is the intrinsic kinetic constant at 25 °C and neutral pH and the two terms k_{25}^{H} and k_{25}^{OH} describe the influence of the activity of H^+ and OH^- on the rate, respectively. $\frac{IAP}{K}$ is the saturation index of the dissolving phase, calculated as the ratio of the ion activity product over the equilibrium constant of the dissolution reaction.

The bentonite studied was estimated to consist of 80% montmorillonite clay with 20% accessory minerals, as previously described in Sect. 2.1 although the specific quantities of the accessory minerals could not be determined. Early efforts to incorporate the kinetic dissolution of one or two (for example, zeolite or mica) into the kinetic model introduced multiple variables. Kinetic rate constants for dissolution at relevant pH are scarcely available in the literature and the model's predicted releases of the ions varied, some ions aligned reasonably well with experimental data, while others did not. Moreover, adjusting the initial abundances of the accessory phases led to significant variations in the model outcomes. Initial model runs with montmorillonite as the sole mineral dissolving indicated that accessory minerals are, in fact, products of montmorillonite alteration. The final model therefore only included a kinetic model for montmorillonite dissolution, with the other minerals considered to be in equilibrium with montmorillonite at every step, both dissolving and precipitating depending on the evolution of the system. Lime was also added as a saturated phase because of its faster dissolution in water compared to montmorillonite. Table 2 shows kinetic parameter values for bentonite and lime from Marty et al. [34]. Initial amounts were 2.94 moles for montmorillonite and 1.3 moles of lime in 0.53 L of water, based on the design mix of the UCS specimens. For this model, montmorillonite's specific surface area (SSA) was measured at 30.4 m^2/g as with the BET method, which is comparable to the values of the Ca-bentonite of De Windt et al. [15]; lime SSA was assumed at 15.5 m^2/g taken from De Windt et al. [15].

Bentonite pore solution analysis indicated the presence of sulfate in solution and hence to account for sulfate in solid phase at $t = 0$ and the observed increases in sulfate concentration over time, gypsum was considered as a dissolving phase alongside bentonite. While the precise form of sulfate in the original bentonite is not known, the addition of lime makes the presence of gypsum as a source phase for sulfate in the mix plausible. The total available amount of SO_3 from XRF results (Table 1) is 0.56% by weight or 0.095 moles per the 2.94 moles of montmorillonite model input. The final model included a lower amount to match the measured sulfate concentrations in solutions, as will be discussed in the relevant section.

Several other potential precipitates were added from the literature [23, 33] as shown in Table S2 in the Supporting Information. Cation exchange was considered for the Na-Ca pair as the major cations in the system, using the built-in Gaines-Thomas formalism [8].

Results and discussion

Strength test results

The UCS of the lime-bentonite system doubled from 300 to over 600 kPa within 7 days and reached 900 kPa by 28 days (Fig. 1a). After that, no significant changes

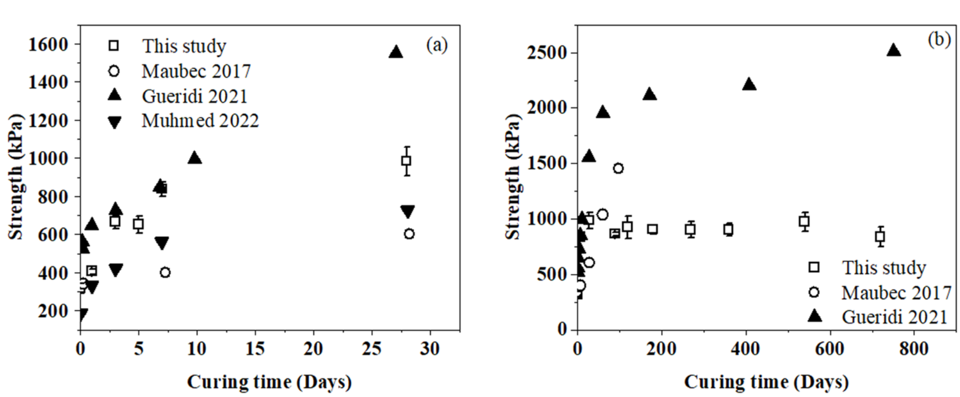

Fig. 1 UCS results of lime-bentonite mix compared to literature data (**a**) up to 28 days and (**b**) up to 720 days of curing

in strength were observed up to 720 days (Fig. 1b). The variation between curing times after 28 days of curing was comparable to the variation between quadruplicate samples for a given curing time, with a ± 20% fluctuation around the average, in the range from 742 to 1046 kPa. For comparison, Fig. 1; Table 3 include studies on lime-treated bentonites with geochemical and mineralogical information as a function of time.

Bandipally et al. [9, 27, 38] studied Na-bentonite with similar geotechnical properties (LL, PL, standard Proctor optimum). Gueridi & Derriche [27] had a significantly higher amount of non-clay minerals such as quartz and feldspars based on chemistry and XRD data, while Muhmed et al. [38] did not report mineralogy, with the chemistry indicating lower amount of silica. Bandipally et al. [9] had Na-montmorillonite with a substantial amount of quartz and traces of kaolinite. Maubec et al. [35] studied a Ca-bentonite with Ca-montmorillonite, some feldspar, quartz and cristobalite.

At 28 days of curing, this study and Muhmed et al. [38] both observed strength gain of + 600 kPa compared to the baseline; Bandipally et al. [9, 27] reported much higher strength gains (+ 1,000–2,000 kPa) at lower or similar lime dosages. Ali & Mohamed [6] reported even higher UCS of + 3,000 kPa at 9% lime. The Ca-bentonite of Maubec et al. [35] showed a slower initial strength increase, only gaining + 300 kPa in the first 28 days. Beyond 28 days, Gueridi & Derriche [27] reported rapid increase to 60 days of curing, reaching almost ~ 2,000 kPa, followed by a slower gain of additional 20% by 820 days. Maubec et al. [35] showed linear increase in strength up to 98 days, gaining ~ 1,000 kPa in strength with 10% lime added. No further increases in strength were observed in the current study.

Differences between the studies can be related to factors including the moisture content of compaction, curing conditions, amount of lime and clay particle size and mineralogy. Bandipally et al. [9] reported an increase in the 28-d UCS of lime-treated bentonite of ~ 250 kPa per percent of lime added, up to 10%, followed by a plateau and eventual decrease at dosages higher than 14%. The lime dosage cannot explain the observed differences between the studies, and the dry unit weight emerged as a likely controlling parameter (Table 3). Another significant difference was that the clay studied by Gueridi and Derriche [27] had higher amounts of non-clay minerals.

Despite the differences in final values between the studies, the rate of strength increase was similar for the first 7 days; the curves started diverging at 28 days, and up to 90 days for the two datasets with available data. The longer dataset of Gueridi and Derriche [27] exhibited a similar trend to our data of the strength tapering off after 90 days. The rate of strength increase may be related to the rate of lime consumption and mineralogical transformations within the systems, as explored in the following sections.

TGA results

The TGA spectrum of the untreated sample (Figure S3) resembled the spectra shown by Guggenheim & Koster Van Groos [28] for Wyoming bentonite SWy-2 and by Földvári [21] for "abnormal" Na-montmorillonites with vacancies in their structure. Other phases are not detectable via TGA in this range, either because there is no mass loss at all (quartz, cristobalite, feldspars) or it occurrs at higher temperatures (mica). Clinoptilolite only exhibits dehydration at about 110ºC [21] and thus could not be distinguished from montmorillonite dehydration.

Quantitative analysis of the cured spectra was performed for three regions (Fig. 2), similar to Maubec et al. [35]: the 100 to 350ºC region corresponds to Calcium Silicate and Aluminate Hydrates, 350 to 410ºC

Table 3 Comparison of bentonite properties in other lime stabilization studies (QL quicklime, SL slaked lime, LL liquid limit, PL plastic limit, OMC optimum moisture Content)

Author	Stabilizer (SL, QL)*	LL, PL* (%)	γ_d, max (kN/m^3)	OMC* (%)	Mineralogy	UCS as cured (kPa)	28-d UCS (kPa)	Treatment conditions
Muhmed et al. [38]	SL 7% 20 and 40˚C	330, 43	11.2	40	Na montmorillonite	65–100	724 (OMC + 40%)	OMC + 10% to + 40%
Gueridi et al. (2021)	QL 5% (75% CaO)	360–450, 45–60	11.76	35	Na montmorillonite, quartz, cristobalite, potassium feldspar, calcite	~ 430	1,560	OMC + 2%
Maubec et al. [35]	QL 10% 20 and 50 ºC	158, 54	11.97	34.8	Ca montmorillonite (83%), feldspar (10%), cristobalite (5%), quartz (2%)	300	600	0.985*OMC
Ali and Mohamed [6]	SL 5 to 25%	320, 43	12.16	40	Na-montmorillonite (other unknown)	500	1,590 (5%), 3,160 (9%)	OMC
Bandipalli et al. (2018)	SL 2–20%	350, 27	n.a.	n.a.	Na-montmorillonite, quartz, kaolinite	290	1,850 (8% SL) 2,400 (10% SL)	OMC
This study	SL 8%	384, 68	11.1	33	Na montmorillonite (~ 80%), quartz, zeolite, cristobalite, feldspar and mica.	317	983	OMC + 7%

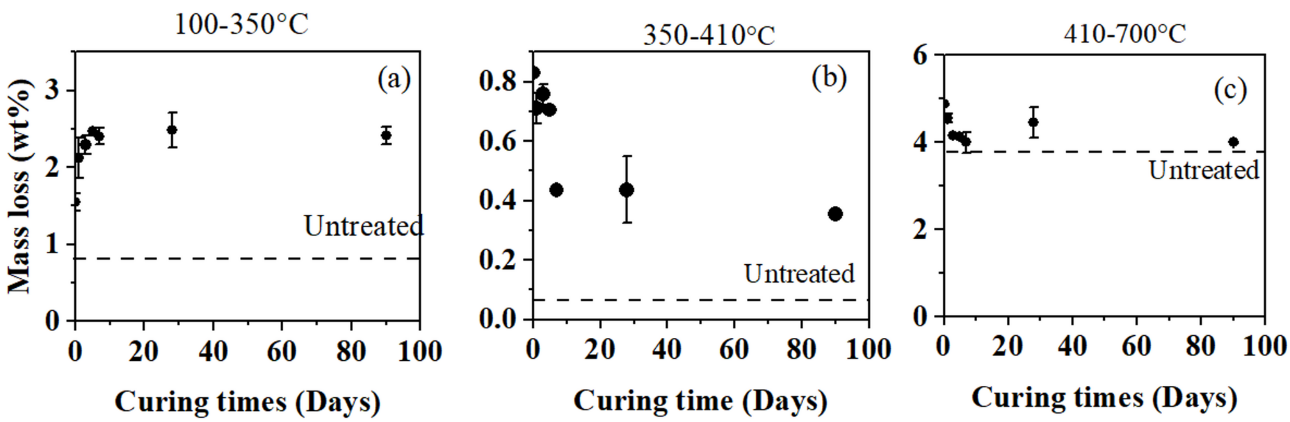

Fig. 2 Mass loss of TGA spectra in three temperature regions as a function of time– dashed lines indicate value in untreated bentonite spectrum

to dehydroxylation of portlandite and 410 to 700°C to dehydroxylation of montmorillonite. A peak split and shift to lower temperatures were observed in this region upon addition of lime, which can be explained by changes in the relative abundance between different types of octahedral sites; weathering was provided by Földvári [21] as one reason for double or low temperature dehydroxylation.

The 100 to 350°C region (Fig. 2a) showed rapid formation of hydrates in the first seven days, followed by a plateau at 2.4%, similar to the value reported by Maubec et al. [35] at 98 days. Vitale et al. [47] also used TGA to study Ca-montmorillonite treated with 3% and 5% CaO and reported 2% mass loss in this region, reached by 28 days of reaction.

The mass loss at 100 to 350°C was accompanied by decreases in both the free lime (Fig. 2b) and the montmorillonite (Fig. 2c) regions, with no further changes up to 90 days of curing. Longer-term data showed some fluctuation in the mass loss, but no significant trends and are thus not shown.

The mass loss in the lime region showed complete consumption by 7 days of curing. Vitale et al. [47] reported no observable free lime via TGA in Ca-montmorillonite treated with 3 and 5% CaO, even in the as-cured mix. Bandipally et al. [9] observed residual free lime via TGA at 28 days only upon addition of 12% lime. Thus, lime consumption by montmorillonite was consistently observed to be a rapid process via TGA analysis.

Plotting the UCS data alongside hydrate formation trends observed in the TGA analysis (Figure S4) showed a direct correlation between strength development and hydrate formation, supporting the relationship between the chemical transformations and the strength gain up to 28 days of curing.

XRD results

XRD spectra are shown in Figure S4. None of the spectra showed any new crystalline phases formed over time, with the exception of portlandite ($Ca(OH)_2$) and calcite ($CaCO_3$). Similarly, Vitale et al. [27, 46] observed no new reflections at lower lime dosages (3 and 5%, respectively). Portlandite reflections were observed up to 5 days of curing, but not at 7 days curing or later times, indicating complete consumption between 5 and 7 days.

Early studies established two main products of lime reaction with montmorillonite: a calcium aluminate hydrate (C_4AH_{13} or $4CaO{\cdot}Al_2O_3{\cdot}13H_2O$) and C-S-H(I), a poorly crystalline tobermorite ($Ca_5Si_6O_{16}(OH)_2{\cdot}4H_2O$) [25]; Diamond & Kinter [17],. Maubec et al. [35] reported the formation of C_4AH_{13} (2θ = 11.2°, d = 7.9 Å) with continuous increase in intensity from 28 to 98 days of curing; Bandipally et al. [9] showed a C-A-H reflection in the same location appearing at 28 days when 12% lime was added, but not at 6% lime. In addition to the low content, observation of this phase in this study was also inhibited due to its overlap with one of the primary clinoptilolite reflections. Maubec et al. [35, 47] reported a diffuse reflection at two-theta 29-30° (d = 3.03 Å) that was attributed to C-S-H formation. This location was within the d-spacing range reported for C-S-H-I (tobermorite-like) gel (3.02–3.06 Å) [25] in lime-stabilized bentonite. However, 3.03 Å is also the location of the primary calcite reflection, and distinguishing between these reflections at low intensities was not possible (Figure S5). The presence of C-A-H and C-S-H could therefore not be ascertained using XRD, which is expected given the low amount and poor crystallinity.

A semi-quantitative analysis for portlandite consumption over time was performed in the spectra obtained from the 8SL and 15SL paste studies by taking the ratio of the height of its reflection to the corundum internal standard (Fig. 3). A relative intensity of 2% corresponded to the background noise. In the 8SL paste, portlandite consumption was a bit slower compared to the UCS break, showing a small portlandite reflection above background at 7 days, and no observable reflection at 10 days. In the 15SL mixture, the relative intensity of portlandite at 4 h

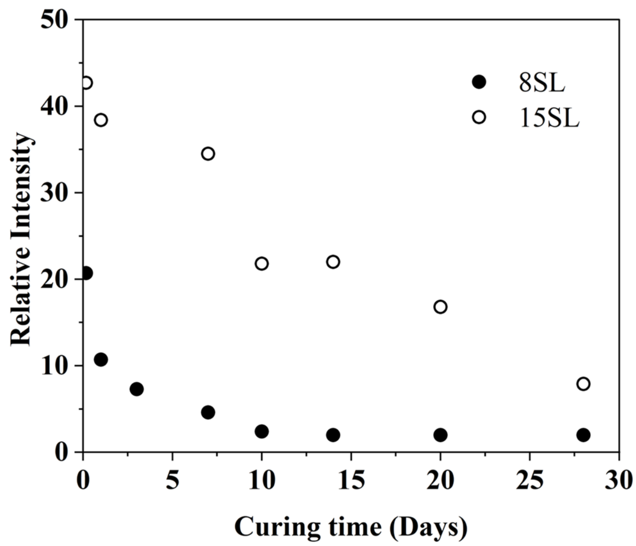

Fig. 3 Portlandite consumption predicted by XRD semi-quantitative analysis

Table 4 Quantitative ^{29}Si NMR analysis of Na-bentonite samples mixed with 8% lime and 40% water

Curing time	Bentonite (Area percentage%)	Hydrate (Area percentage%)
0	93.21	6.79
5	91.73	8.27
7	79.90	20.09
28	60.89	39.10

curing was approximately double and persisted in the mixture up to 28 days, when the paste study was terminated; this result is consistent with Bandipally et al. [9]. In both cases, the decrease in intensity followed a logarithmic trend with time. This data will be further discussed in the context of the kinetic model.

NMR results

The NMR analysis of the untreated Na-bentonite (Figure S6) was performed with reference to Lippmaa et al. [30]. Five peaks were observed in the spectrum, in agreement with XRD. Montmorillonite peak is the main peak at -83.3 ppm (Q^3), with additional phases assigned to anorthite (feldspar) (Q^2) at -79 ppm, muscovite (Q^3) at -80 ppm and silica polymorphs (Q^4) quartz and cristobalite, located at -98 ppm.

Na-bentonite spectra for short term curing (0 to 28 days) are shown in Figure S7 and quantitative analysis in Table 4. A new peak appeared at -76 ppm in the treated samples, assigned to calcium silicate hydrate (C-S-H) [41]. Quantitative analysis showed a gradual increase in the C-S-H and decrease in other peak areas (montmorillonite and accessory minerals). After 28 days of curing no meaningful trend was observed in the long-term data (Figure S8).

Solution composition

Figure 4 shows key elements in solution up to 720 days and Figure S9 shows the same graphs up to 90 days of curing for clarity. Substantial fluctuations were observed in most parameters, reflected both in the standard deviations at each curing time and in the long-term trends. This is attributed to the low amount of recovered solution, which both complicates analysis and increases variability. For this reason, trends are best evaluated in conjunction with the modeling results that place the data into the context of the reactions controlling solution composition.

Geochemical model

The first model run using the kinetic rate constants in Table 2 showed complete lime consumption within one day and pH drop to 12.3 within three days. These trends do not reflect the experimental data, as solid analysis from both TGA and XRD showed that portlandite persisted in the system up to five days of curing and solution data indicated pH higher than 12.3 up to seven days of curing. A sensitivity analysis was therefore conducted by varying the rate constant associated with the influence of OH- activity in solution (-logk25OH) from 10.4 to 12 to determine the optimal value that would best match the model predictions with the experimental data.

For any given rate, the system reached equilibrium after 1.08 moles (37% of the initial 2.94 moles) of montmorillonite were dissolved. The time to reach equilibrium depends on the specific rate constant, as shown in Fig. 5, and ranges from 120 days for the fastest rate (pk_{OH} 10.4) to 3,420 days for the slowest rate (pk_{OH} 12). The solution composition and phase assemblage are identical for all rates when plotted as a function of the amount of montmorillonite dissolved and shown in Figs. 6 and 7, respectively. Mg-bearing precipitates are shown in Figure S10.

The trends in the evolution of pore solution composition and corresponding solid phase assemblage can be summarized in four stages, as shown in Table 5. The first stage up to 0.1 mol of montmorillonite dissolution involved rapid portlandite consumption and formation of C-S-H, C-A-H and C-A-S-H (stratlingite). Progressive dissolution released further Mg, Si and Al and shifted phase stability, with Ca-poor tobermorite-II replacing Ca-rich jennite and stratlingite. After 0.33 moles of montmorillonite were dissolved, tobermorite-II also started dissolving, in favor of the formation of silicates that are montmorillonite alteration products such as albite, chlorite and talc. Ettringite was predicted to form again in this final stage. Sulfate-bearing phase stability was sensitive to the amount of gypsum used in the input, which in

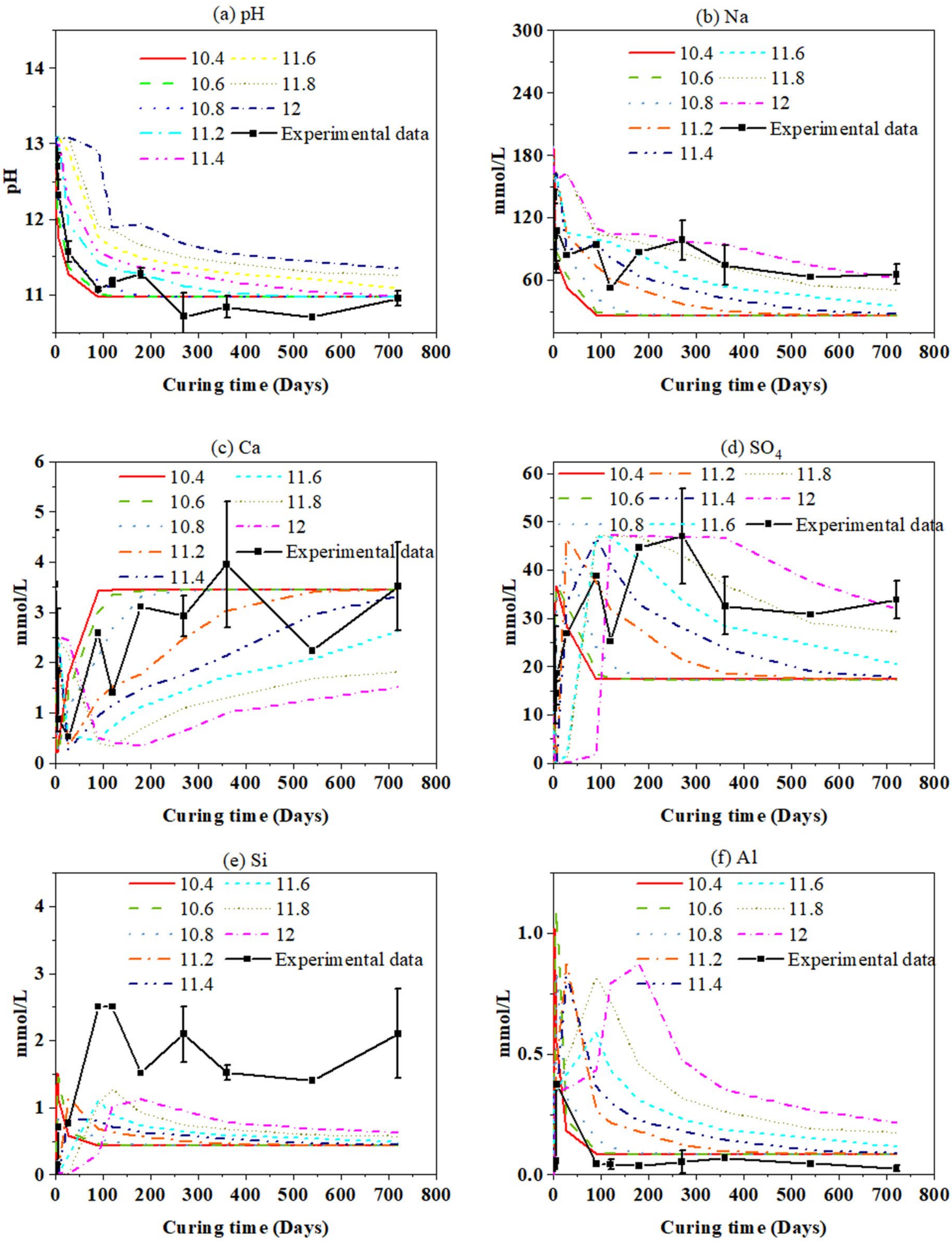

Fig. 4 Experimental solution composition and model prediction as a function of curing time

this case was 0.03 moles. As previously noted, the total amount of sulfate based on XRF is 0.095 moles; however, given that only a third of the total amount of montmorillonite was predicted to dissolve at equilibrium, it is also logical to consider lower available amount of sulfate in the system.

The model output was converted from units of montmorillonite dissolved to units of time for each pk_{OH}

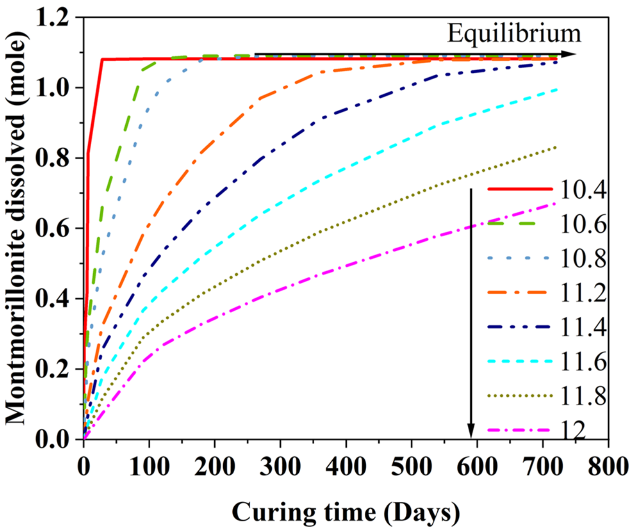

Fig. 5 Modeled data of montmorillonite reacted over time at different–$logk_{25}^{OH}$ rates

resulting in distinct curves plotted in Fig. 4. There was no single rate that yielded good agreement between the experimental data and model output for all parameters. Specifically, pH, Ca and Al were predicted fairly well by pk_{OH} 10.8 across the entire time frame. Silica in solution was also predicted well by 10.8 up to 28 days (Figure S8), whereby later times showed an overall trend that better matched slower rates of 11.6 to 11.8. Na and SO_4 curves both agreed with faster rates of 10.4 to 10.6 in the first 7 days, then progressively matched slower and slower rates up to 11.8–12 by 720 days of curing.

Portlandite consumption observed from XRD analysis versus the curves predicted by the model is shown in Fig. 8, showing an alignment at pk_{OH} 11.2. Similar to the lime-kaolinite model discussed in Ahmadullah & Chrysochoou [1], this model also predicted faster consumption of lime compared to the decrease of Ca concentration in solution. In other words, no kinetic rate could predict for which both the solution composition (pH, Ca) and solid observations (XRD, TGA). This was true for both the lime-kaolinite system studied by Ahmadullah and Chrysochoou [1] and the lime-montmorillonite system in this study. In both cases, portlandite dissolution was predicted to be slower compared to the decrease of the solution parameters (pH, Ca). This implies that the released Ca^{2+} and OH^- are consumed by phases other than the ones predicted by the model. Given that Al^{3+} is better predicted by faster dissolution and SO_4^{2-} and Si by slower dissolution, it appears likely that the formation of C-A-H metastable phases may account for this phenomenon.

Given all these observations, the first three stages of montmorillonite dissolution may be accounted for as follows:

1. S1 (0-0.1 moles): this stage corresponded to the time it took for portlandite to be fully consumed, with a rapid decrease in Ca and Na concentrations. Given the XRD, TGA and solution data, this stage corresponded to between 5 and 7 days of curing.
2. S2 (0.1–0.25 moles): During this stage, the modeled Si concentration in solution increased as tobermorite replaced jennite; the experimental data point to this stage occurring at 5 to 7 days of curing. A clear distinction between the end point of phase S1 and beginning of phase S2 cannot be made based on the experimental data, but the end of phase S2 may be reasonably set at 7 days.
3. S3 (0.25–0.33 moles): Ca in solution continued to decrease to reach a plateau and C-S-H formation reached its maximum; this point corresponded to the maximum strength and the minimum Ca in solution at 28 days. This correlation between strength development and C-S-H formation is also shown in Figure S4.

During the initial 90 days, the cementitious phases primarily control solubility of the measured parameters in solution. Given the observed trends in solution, it appeared likely that cementitious reactions were completed within 90 days of curing, as predicted by a pk_{OH} value of 10.8, which is also close to the literature value of 10.6. Further fluctuations in the system have no bearing

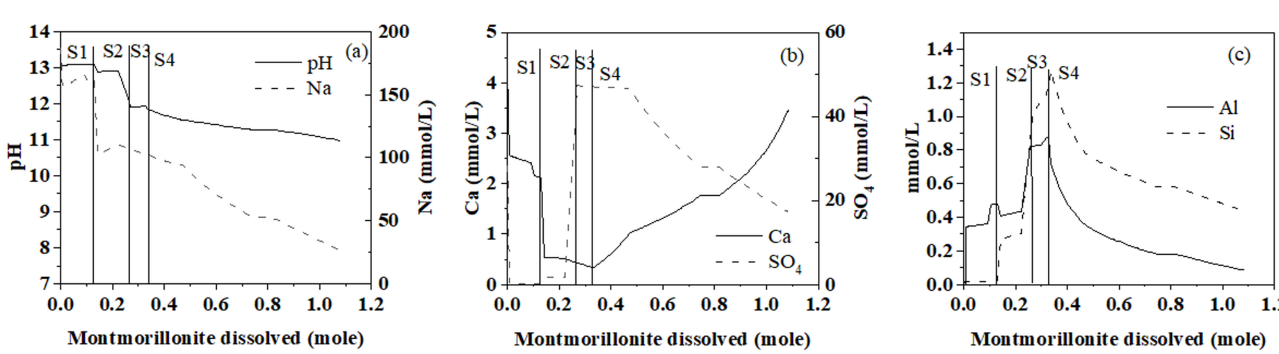

Fig. 6 Model prediction of solution composition as a function of dissolved montmorillonite (Stages S1 through S4 are described in Table 3)

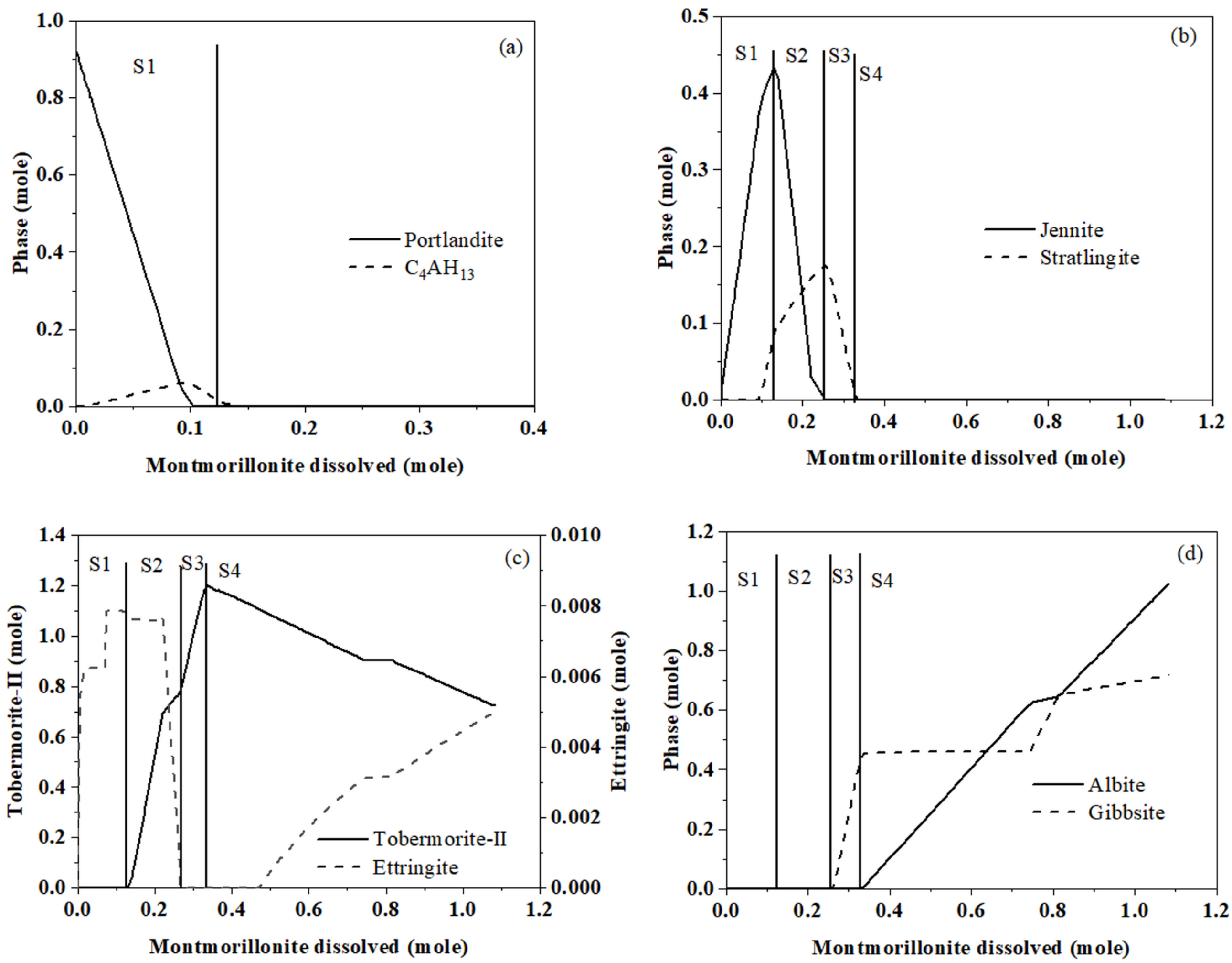

Fig. 7 Model prediction of solid phases as a function of dissolved montmorillonite (Stages S1 through S4 are described in Table 3)

Table 5 Summary of the model stages in the evolution of pore solution composition and phase assemblage

Stage	Moles of montmorillonite dissolved	Solution trends	Solid phase trends
S1	**0-0.1**	pH constant at 13. Na, Ca and SO_4 decreased. Al and Si increased.	Portlandite was fully consumed. Jennite, ettringite, stratlingite and hydrotalcite formed. C_4AH_{13} formed and dissolved.
S2	**0.1–0.25**	pH decreased to 11.9. Na and Ca decreased. Si, Al, SO_4 increased.	Jennite, hydrotalcite and ettringite became zero. Tobermorite-II, gibbsite, chlorite and K-mica started forming. Ettringite started dissolving.
S3	**0.25–0.33**	pH plateaued at 11.9. Na and Ca decreased. SO_4 plateaued. Al and Si increased.	Stratlingite became zero. Tobermorite-II became maximum. Chlorite and K-mica increased. Gibbsite formed.
S4	**0.33–1.1**	pH decreased to 10.96. Na, Al and Si decreased. Ca increased. SO_4 decreased at 0.5 moles of montmorillonite dissolved.	Tobermorite-II decreased. Stratlingite became zero. Ettringite formed at 0.5 moles of montmorillonite dissolved. K-mica plateaued. At 0.7 moles of montmorillonite dissolved, talc formed and chlorite decreased. Gibbsite increased.

on the measured strength and are attributed to experimental variability. During stage 4, silicate phases and continuous weathering of montmorillonite were primarily responsible for the observed changes in solution. The model does not consider the influence of all accessory minerals that were also present in the system simultaenously, most notably Na-clinoptilolite. As noted in the model description, accessory minerals were predicted to form as montmorillonite alteration products; however, the model could not capture the presence of all of them at once. When Na-clinoptiolite was considered as one of the equilibrium phases instead of albite, Si concentration was predicted by the model accurately at longer curing times (Figure S11). No changes in UCS were observed at

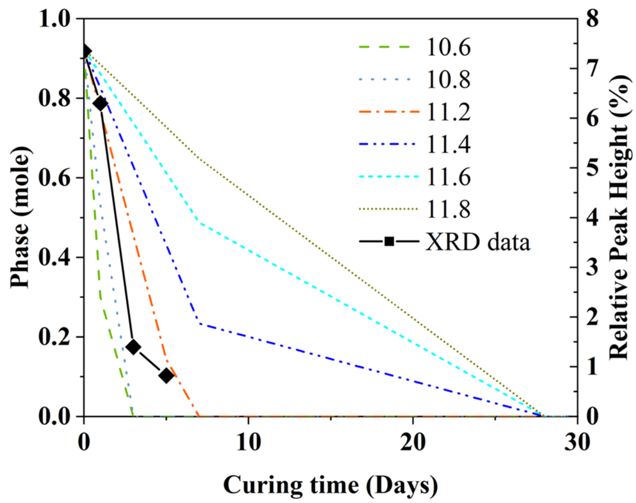

Fig. 8 Portlandite consumption over time at different pkOH values compared to values obtained by semi quantitative XRD

longer time frames, indicating that further weathering of montmorillonite and conversation to other silicates did not influence long-term strength.

Conclusions

The spectroscopic and pore solution study of a Na-bentonite clay reacting with lime over 720 days showed that the evolution of the system could be described with a kinetic model that accounted for most observed data with a single kinetic rate up to 90 days of curing. The evolution of reactions was predicted by the model as follows:

1. In the beginning portlandite was consumed rapidly which decreased pH and Ca concentration up to 7 days of curing, verified by solution data. The model predicted the formation of C-S-H (jennite), C-A-H (e.g., C_4AH_{13}), calcium alumino-silicate hydrate (C-A-S-H) such as stratlingite, and hydrotalcite. Portlandite was fully consumed within 7 days which was confirmed from TGA and XRD analysis.
2. After 7 days jennite and stratlingite were predicted to transform into tobermorite-II. The experimental data could not corroborate specific phases in the solid but showed a decrease in pH and increase in strength up to 28 days that were in alignment with model predictions.
3. After 28 days and up to 90 days, montmorillonite dissolution continued to occur, with the model predicting formation of small amounts of ettringite, some tobermorite dissolution, and formation of secondary minerals such as albite and talc. Similarly, these transformations could not be experimentally verified as the spectroscopic analyses did not show any meaningful trends past 90 days. No impact on long term strength was observed either.

   Experimental data in solution confirmed that equilibrium was reached within 90 days, with little changes in solution after that time point.

In terms of implications for practical applications, ninety days is a short period of time in the context of clay stabilization applications. However, current design specifications for lime stabilized clays in road construction utilize 28-day strength as the design parameter, and this is based on the time frame of cement hydration. The kinetic models for lime interaction with different clay minerals can be used to predict time frames for equilibrium depending on the mineralogy and amount of lime used and accordingly inform the design and long-term testing protocol for the system. In future studies, other parameters may be incorporated in the model, for example the effect of long-term carbonation on the mineralogy and strength of the material, or external attacks by chloride or sulfate. Further improvements to the model can include more accurate modeling of accessory minerals, incorporation of solution chemistry in the rate model and considerations of rate limiting reactions.

TABLES.

Supplementary Information

The online version contains supplementary material available at https://doi.org/10.1186/s12932-025-00103-4.

Supplementary Material 1

Acknowledgements
This work has been supported by the National Science Foundation, grant number 1740554. The authors are grateful for the assistance of Leana Santos, Corey Walker, Caitlin Jenkins, Samuel Pontes and Kayla Turner in the laboratory analyses.

Author contributions
TA- Conceptualization, experimental analysis, data analysis, modeling, original draft preparation and editingMC-Funding acquisition, conceptualization, data curation, modeling, draft editing.

Funding
This project was supported by the National Science Foundation, NSF project number 1740554.

Data availability
No datasets were generated or analysed during the current study.

Declarations

Ethics approval and consent to participate
Not applicable.

Consent to publish
Not applicable.

Competing interests
The authors declare no competing interests.

Received: 24 February 2025 / Accepted: 12 July 2025
Published online: 30 July 2025

References

1 Ahmadullah T, Chrysochoou M (2023) Thermodynamic and kinetic modeling of the Lime–Kaolinite system. ACS Earth Space Chem 7(10):1947–1955. https://doi.org/10.1021/acsearthspacechem.3c00085
2 Ahmadullah T, Chrysochoou Maria (2022) &. Strength Development and Reaction Kinetics in Lime-Treated Clays. In *Geo-Congress 2022* (pp. 138–147). https://doi.org/10.1061/9780784484012.014
3 Akula P, Hariharan N, Little DN, Lesueur D, Herrier G (2020) Evaluating the Long-Term durability of lime treatment in hydraulic structures: case study on the Friant-Kern Canal. Transp Res Rec 2674(6):431–443. https://doi.org/10.1177/0361198120919404
4 Akula P, Little DN (2020) Analytical tests to evaluate pozzolanic reaction in lime stabilized soils. MethodsX 7:100928. https://doi.org/10.1016/j.mex.2020.100928
5 Akula P, Naik SR, Little DN (2021) Evaluating the durability of Lime-Stabilized soil mixtures using soil mineralogy and computational geochemistry. Transp Res Rec 2675(9):1469–1481. https://doi.org/10.1177/03611981211007848
6 Ali H, Mohamed M (2019) Assessment of lime treatment of expansive clays with different mineralogy at low and high temperatures. Constr Build Mater 228:116955. https://doi.org/10.1016/j.conbuildmat.2019.116955
7 Al-Mukhtar M, Lasledj A, Alcover J-F (2010) Behaviour and mineralogy changes in lime-treated expansive soil at 20°C. Appl Clay Sci 50(2):191–198. https://doi.org/10.1016/j.clay.2010.07.023
8 Appelo CAJ, Postma D (2004) Geochemistry, groundwater and pollution. CRC
9 Bandipally S, Cherian C, Arnepalli DN (2018) Characterization of Lime-Treated bentonite using thermogravimetric analysis for assessing its Short-Term strength behaviour. Indian Geotech J 48(3):393–404. https://doi.org/10.1007/s40098-018-0305-7
10 Bell FG (1996) *Lime stabilization of clay minerals and soils*. *42*(4), 223–237. https://doi.org/10.1007/s10706-017-0392-8
11 Chakraborty S, Nair S (2020) Impact of curing time on moisture-induced damage in lime-treated soils. Int J Pavement Eng 21(2):215–227. https://doi.org/10.1080/10298436.2018.1453068
12 Chipera SJ, Bish DL (2001) Baseline studies of the clay minerals society source clays: powder X-Ray diffraction analyses. Clays Clay Miner 49(5):398–409. https://doi.org/10.1346/CCMN.2001.0490507
13 Chittoori Bhaskar CS, Puppala Anand J, Pedarla Aravind (2018) Addressing clay mineralogy effects on performance of chemically stabilized expansive soils subjected to seasonal wetting and drying. J Geotech GeoEnviron Eng 144(1):04017097. https://doi.org/10.1061/(ASCE)GT.1943-5606.0001796
14 Chrysochoou M (2014) Investigation of the mineral dissolution rate and strength development in stabilized soils using quantitative X-Ray diffraction. J Mater Civ Eng 26(2):288–295. https://doi.org/10.1061/(ASCE)MT.1943-5533.0000814
15 De Windt L, Deneele D, Maubec N (2014) Kinetics of lime/bentonite pozzolanic reactions at 20 and 50°C: batch tests and modeling. Cem Concr Res 59:34–42. https://doi.org/10.1016/j.cemconres.2014.01.024
16 Delage P, Cui YJ, Tang AM (2010) Clays in radioactive waste disposal. J Rock Mech Geotech Eng 2(2):111–123. https://doi.org/10.3724/SP.J.1235.2010.00111
17 Diamond S, Kinter EB (1965) Mechanisms of soil-lime stabilization. 92:83–102
18 Eades JL, Ralph G E (1960) Reaction of hydrated lime with pure clay minerals in soil stabilization. Highway Res Board 262:51–63
19 Estabragh AR, Kholoosi MM, Ghaziani F, Javadi AA (2017) Stabilization and solidification of a clay soil contaminated with MTBE. J Environ Eng 143(9):04017054. https://doi.org/10.1061/(ASCE)EE.1943-7870.0001248
20 Fernández AM, Cuevas J, Rivas P (2000) Pore Water Chemistry of the Febex Bentonite. *MRS Proceedings*, *663*, 573. https://doi.org/10.1557/PROC-663-573
21 Földvári M (2011) Handbook of thermogravimetric system of minerals and its use in geological practice, vol 213. Geological Institute of Hungary Budapest
22 Harrison G, H., Davidson D (1960) *Lime fixation in clayey soils*. *262*, 20–32
23 Gaucher EC, Blanc P (2006) Cement/clay interactions– A review: experiments, natural analogues, and modeling. Mech Model Waste/Cement Interact 26(7):776–788. https://doi.org/10.1016/j.wasman.2006.01.027
24 Gherardi F, Audigane P, Gaucher EC (2012) Predicting long-term geochemical alteration of wellbore cement in a generic geological CO2 confinement site: tackling a difficult reactive transport modeling challenge. J Hydrol 420–421:340–359. https://doi.org/10.1016/j.jhydrol.2011.12.026
25 Glenn GR, Handy R (1963) Lime-clay mineral reaction products. Highway Res Rec, *29*
26 Goldberg I, Alexander K (1953) Some effects of treating expansive clays with calcium hydroxide. In Symposium on Exchange Phenomena in Soils. In *Symposium on Exchange Phenomena in Soils*. ASTM International
27 Gueridi F, Derriche Z (2021) Strength development and lime consumption progress relationship in lime stabilized bentonite samples. Bull Eng Geol Environ 80(7):5505–5514. https://doi.org/10.1007/s10064-021-02262-x
28 Guggenheim S, Van Koster AF (2001) Baseline studies of the clay minerals society source clays: thermal analysis. Clays Clay Miner 49(5):433–443. https://doi.org/10.1346/CCMN.2001.0490509
29 Lasaga AC (1981) Transition state theory. *Rev. Mineral.;*(United States), *8*
30 Lippmaa E, Maegi M, +, Samoson A, Engelhardt G, Grimmer A (1980) Structural studies of silicates by solid-state high-resolution silicon-29 NMR. J Am Chem Soc 102(15):4889–4893
31 Little DN (2012) Lime Stabilization of Subgrade Soils for Structural Purposes: Past Evidence and Future Needs. In M. L. Thomson & J. H. Brisch (Eds.), *Lime*: Building on the 100-Year Legacy of The ASTM Committee C07 (Vols. STP1557-EB, p. 0). ASTM International. https://doi.org/10.1520/STP20120022
32 Locat J, Berube M-A, Choquette M (1990) *Laboratory investigations on the lime stabilization of sensitive clays: Shear strength development*. *27*, 294–304. https://doi.org/10.1139/t90-040
33 Lothenbach B, Winnefeld F (2006) Thermodynamic modelling of the hydration of Portland cement. Cem Concr Res 36(2):209–226. https://doi.org/10.1016/j.cemconres.2005.03.001
34 Marty NCM, Claret F, Lassin A, Tremosa J, Blanc P, Madé B, Giffaut E, Cochepin B, Tournassat C (2015) A database of dissolution and precipitation rates for clay-rocks minerals. Appl Geochem 55:108–118. https://doi.org/10.1016/j.apgeochem.2014.10.012
35 Maubec N, Deneele D, Ouvrard G (2017) Influence of the clay type on the strength evolution of lime treated material. Appl Clay Sci 137:107–114. https://doi.org/10.1016/j.clay.2016.11.033
36 Moh Z-C (1965) Reactions of soil minerals with cement and chemicals. Highway Res Rec, *86*
37 Mower TE (1994) Pore-water extraction from unsaturated tuff using triaxial and one-dimensional compression methods, nevada.test site, nevada. Denver, Colorado, vol 93. US Department of the Interior, US Geological Survey
38 Muhmed A, Mohamed M, Khan A (2022) The impact of moisture and clay content on the unconfined compressive strength of lime treated highly reactive clays. Geotech Geol Eng 40(12):5869–5893. https://doi.org/10.1007/s10706-022-02255-x
39 Parkhurst DL, Appelo C (2013) Description of input and examples for PHREEQC version 3—A computer program for speciation, batch-reaction, one-dimensional transport, and inverse geochemical calculations. US Geol Surv Techniques Methods 6(A43):497
40 Pedarla A, Chittoori S, Puppala AJ (2011) Influence of mineralogy and plasticity index on the stabilization effectiveness of expansive clays. Transp Res Rec 2212(1):91–99. https://doi.org/10.3141/2212-10
41 Pomakhina E, Deneele D, Gaillot A-C, Paris M, Ouvrard G (2012) 29Si solid state NMR investigation of pozzolanic reaction occurring in lime-treated Ca-bentonite. Cem Concr Res 42(4):626–632. https://doi.org/10.1016/j.cemconres.2012.01.008
42 Puppala AJ (2016) Advances in ground modification with chemical additives: from theory to practice. Transp Geotechnics 9:123–138. https://doi.org/10.1016/j.trgeo.2016.08.004
43 Rumman R, Bari MS, Manzur T, Kamal MR, Noor MA (2020) A durable concrete mix design approach using combined aggregate gradation bands and rice husk Ash based blended cement. J Building Eng 30:101303. https://doi.org/10.1016/j.jobe.2020.101303
44 Tabet Wassim E, Cerato Amy B, Madden Andrew E S., Jentoft Rolf E (2018) Characterization of hydration products' formation and strength development in Cement-Stabilized kaolinite using TG and XRD. J Mater Civ Eng 30(10):04018261. https://doi.org/10.1061/(ASCE)MT.1943-5533.0002454
45 Tabet Wassim E, Cerato Amy B, Jentoft Rolf (2017) &. The Use of Thermogravimetry in Quantifying the Hydration Products in Cement-Stabilized Kaolinite. In *Geotechnical Frontiers 2017* (pp. 92–102). https://doi.org/10.1061/9780784480472.010
46 Vitale E, Deneele D, Paris M, Russo G (2017) Multi-scale analysis and time evolution of pozzolanic activity of lime treated clays. Appl Clay Sci 141:36–45. https://doi.org/10.1016/j.clay.2017.02.013
47 Vitale E, Deneele D, Russo G (2016) Multiscale analysis on the behaviour of a lime treated bentonite. Procedia Eng 158:87–91. https://doi.org/10.1016/j.proeng.2016.08.410

48 Vollpracht A, Lothenbach B, Snellings R, Haufe J (2016) The pore solution of blended cements: A review. Mater Struct 49(8):3341–3367. https://doi.org/10.1617/s11527-015-0724-1
49 Weise K, Ukrainczyk N, Koenders E (2021) A mass balance approach for thermogravimetric analysis in pozzolanic reactivity R3 test and effect of drying methods. Materials 14(19). https://doi.org/10.3390/ma14195859

Publisher's note